A Hierarchical Model for Aggregated Functional Data

Ronaldo Dias, Nancy L. Garcia *

Department of Statistics, University of Campinas (UNICAMP), Brazil

and

Alexandra M. Schmidt

Department of Statistics, IM-UFRJ, Brazil

October 1, 2018

Abstract

In many areas of science one aims to estimate latent sub-population mean curves based only on observations of aggregated population curves. By aggregated curves we mean linear combination of functional data that cannot be observed individually. We assume that several aggregated curves with linear independent coefficients are available. More specifically, we assume each aggregated curve is an independent partial realization of a Gaussian process with mean modeled through a weighted linear combination of the disaggregated curves. We model the mean of the Gaussian processes as a smooth function approximated by a function belonging to a finite dimensional space $\mathcal{H}_K$ which is spanned by K B-splines basis functions. We explore two different specifications of the covariance function of the Gaussian process: one that assumes

1

a constant variance across the domain of the process, and a more general variance structure which is itself modelled as a smooth function, providing a nonstationary covariance function. Inference procedure is performed following the Bayesian paradigm allowing experts' opinion to be considered when estimating the disaggregated curves. Moreover, it naturally provides the uncertainty associated with the parameters estimates and fitted values. Our model is suitable for a wide range of applications. We concentrate on two different real examples: calibration problem for NIR spectroscopy data and an analysis of distribution of energy among different type of consumers.

Keywords: Bayes' theorem; B-splines; Covariance function; Gaussian process.

1 Introduction

The problem we address is the estimation of latent sub-population mean and covariance curves when only populational aggregated data is available. By aggregated data we mean that each sample consists of linear combinations of functional data that cannot be observed individually for each sub-population.

Certainly, there are many methods of fitting curves to data. A collection of techniques known as nonparametric regression, for example, allows great flexibility in the possible form of the regression curve α. In particular, it assumes no parametric form for it. In fact, a nonparametric regression model only makes the assumption that the regression curve belongs to some infinite collection of curves. Consequently, in order to propose a nonparametric model one may just need to choose an appropriate space of functions where he/she believes that the regression curve lies. This choice, usually, is motivated by the degree of smoothness of α. Then, one uses the data to determine an element of this function space that can represent the unknown regression curve. Consequently, nonparametric techniques rely more heavily on the data for information about α than their parametric counterparts. Also, this flexibility on the form of the curve allows one to incorporate prior information. The literature on nonparametric regression is vast, for the interested reader we refer to the book of Eubank (1999).

The set up for nonparametric regression assumes that an unknown function α of one or more variables and a set of measurements $y_1, \ldots, y_n$ are such that:

$$y_i = \mathcal{L}_i \alpha + \varepsilon_i,$$

where $\mathcal{L}_1, \ldots, \mathcal{L}_n$ are linear functionals defined on some linear space $\mathcal{H}$ containing α, and $\varepsilon_1, \ldots, \varepsilon_n$ are measurement errors usually assumed to be independent, with common, zero mean normal distributions with unknown variance σ^2. Typically, the $\mathcal{L}_i$ will be point evaluations of the function α. That is, $\mathcal{L}_i g = g(x_i)$ and $y_i = y(x_i)$, where x_i are the explanatory variables for $i = 1, \ldots, n$.

The problem we address here is more general. We have several unknown functions $\alpha_c, c = 1, \ldots, C$ of one or more variables and the set of measurements are given by

$$y_i = \sum_{c=1}^{C} \mathcal{L}_{ic} \alpha_c + \varepsilon_i \tag{1.1}$$

3

where $\mathcal{L}_{ic}, i = 1, \ldots, I, c = 1, \ldots, C$ are the linear functionals. The problem is to estimate the functions $\alpha_c, c = 1, \ldots, C$ based on the measurements $y_i, i = 1, \ldots, I$.

More specifically, in our model we assume each aggregated curve y_i is an independent partial realization of a Gaussian process with mean modeled through a weighted linear combination of the disaggregated curves α_cs. Following Dias, Garcia and Martarelli (2009) we model the mean of the Gaussian process as a smooth function approximated by a function belonging to a finite dimensional space $\mathcal{H}_K$ which is spanned by K B-splines basis functions. This is not the only choice, other basis could be used such as Fourier expansion, wavelets, natural splines. See, for example, Silverman (1986), Kooperberg and Stone (1991), Vidakovic (n.d.), Dias (1998) and Dias (2000).

In this work, differently from Dias et al. (2009), we consider two different structures for the covariance function of the Gaussian process postulating models that impose positive definiteness condition on the function. The first one assumes a uniform structure across the domain of the process, the second one models the covariance itself as a smooth function providing a nonstationary behaviour. Our model is going to be applied for two practical situations. In both of them it is reasonable to consider that the experts in the field have prior information on the disaggregated curves. Therefore, in order to incorporate this opinion, inference procedure will be performed following the Bayesian paradigm. As a by-product, we naturally obtain the uncertainty associated with the parameters estimates, and fitted values.

This paper is organized as follows. Section 2 presents two motivating examples: calibration problem for NIR spectroscopy data and an analysis of distribution of energy among different types of consumers. Section 3 describes our proposed hierarchical model to estimate latent disaggregate curves when only aggregated population observations are available. Therein we also propose a non-stationary covariance function allowing the variance of the underlying process to smoothly change across the domain of the function. Next section analyzes different sets of artificial data. The aim is to check the ability of the model in recovering the true disaggregated functions under different scenarios. Then Section 5 discusses the analysis for the two motivating examples described in subsections 2.1 and 2.2. Finally, Section 6 concludes.

2 Motivating examples

2.1 Near-infrared (NIR) spectroscopy data: a calibration problem

Analyzing materials to determine their chemical composition is a basic tool of science. It is used in many applications such as food safety testing, protein detection, pharmaceutical purposes, forensics, to mention just a few. This analysis can be done directly in the laboratory by usually expensive and time-consuming techniques. An alternative is to determine the chemical composition through NIR spectroscopy which is a low cost technique, relatively simple to use and provides adequate accuracy in many practical situations. Some references with practical applications of NIR spectroscopy are Candolfi, De Maesschalck, Massart, Hailey and Harrington (1999); Rodriguez-Saona, Khambaty, Fry and Calvey (2001); Maraboli, Cattaneo and Giangiacomo (2002); Tewari, Mehrotra and Irudayaraj (2003); Cozzolino, Flood, Bellon, Gishen and De Barros Lopes (2006); Schönbrodt, S., Winter and G. (2006); Saranwong and Kawano (2008a, 2008b); Woodcock, O'Donnell and Downey (2008); Botonjic-Sehic, Brown, Lamontagne and Tsaparikos (2009); and Romía and Bernárdez (2010). For introductory material on the subject see Shenk and Westerhaus (1991), Brereton (2003), and Burns and Ciurczac (2007).

When atoms or molecules absorb light, the energy input excites a quantized structure to a higher energy level. The type of excitation depends on the wavelength of the light. NIR spectroscopy technology is based on the fact that each of the major chemical components of a sample has near infrared red absorption properties in the region 700-2500 nm. An absorption spectrum is the absorption of light as a function of wavelength. The NIR spectrum of a sample is the summation of these absorption properties for each chemical sample resulting in a continuous curve measured by modern scanning instruments at hundreds of equally spaced wavelengths. The information contained in this curve can be used to predict the chemical composition of the sample. The problem lies in extracting the relevant information from possibly thousands of overlapping peaks. This can be accomplished by applying the Beer-Lambert Law. The Beer-Lambert law is the linear relationship between absorbance and concentration of absorbing species.

Analysing a training set of different samples with distinct compositions allow us to calibrate the analysis. Osborne, Fearn, and Hindle (1993) described applications in food analysis and reviewed some of the standard approaches to the calibration problem. Multivariate calibration techniques

are widely used in the literature for this kind of problem. We propose a different approach by treating this problem in the framework of functional data analysis. We regard the response of interest as an aggregated continuous curve observed only at a set of discrete points. Therefore, having measurements of the NIR spectrum for several chemical samples, with distinct compositions, will allow us to estimate the typical curve for each constituint of the sample. Figure 2.1 shows the absorbance curves measured for a dataset of 10 polyaromatic hydrocarbons (PAH) obtained by Electronic Absorption Spectroscopy. The sample consists of 25 chemical samples, each sample composed of varying compositions of 10 different constituents (pyrene, acenaphthene, anthracene, acenaphthylene, chrysene, benzanthracene, uoranthene, uorene, naphthalene, phenanthracene). Each sample was submitted to 27 wavelengths (220nm–350nm). This dataset was presented by Brereton (2003) to illustrate multivariate calibration techniques.
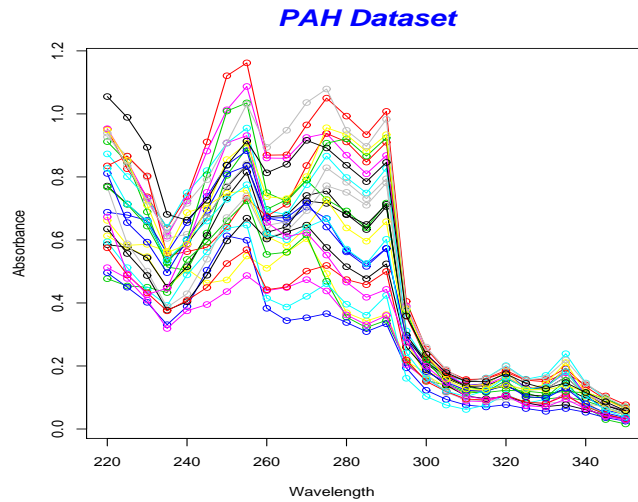

Figure 2.1: Polyaromatic hydrocarbons spectra

2.2 Electric load

The distribution of electric energy is done in several stages: first substations provide energy for regions in the city. This energy arrives at power transformers (*trafo*, an usual acronym for transformer) that redistributes it to micro-regions. Each micro-region is composed of different types of consumers, residential, commercial, industrial, among others. For each type of consumer, there are

peaks of consumption at certain hours of the day. In Brazil, for example, it is empirically known that residential consumers have a peak on energy consumption between 6–8pm (due partially to the use of electric showers) and commercial and industrial consumers have their peak between 8am–6pm. To avoid overload, trafos have to be designed to deal with the maximum load of the day. Ideally, the distribution of electric energy should be done in such a way that there is a constant load during the whole day, all days of the week, all over the year for all power plants, substations and transformers. Therefore, to have a more efficient and uniform distribution of electricity, it is necessary to know the profile of the consumption for each type of consumer. For each type of consumer, this typical curve is called the *typology*. The empirical evidence described before might be used as prior information when modeling the typology for each type of consumer.

From a practical point of view, it is very difficult and expensive to obtain samples from individual consumers. Commonly, the data available are aggregated data from power transformers (trafos). Typically each trafo comprises around 50 consumers. Notice that this data is the sum of all load demanded by the *market* (the number of consumers of each type) of this trafo. Moreover, due to billing issues, the market of each trafo is known. Therefore, having measurements of the electric load for several different trafos, with distinct markets, provides us with the information to estimate the individual curves for each type of consumer. Figure 2.2 shows the data from two trafos, that we analyse in Section 2
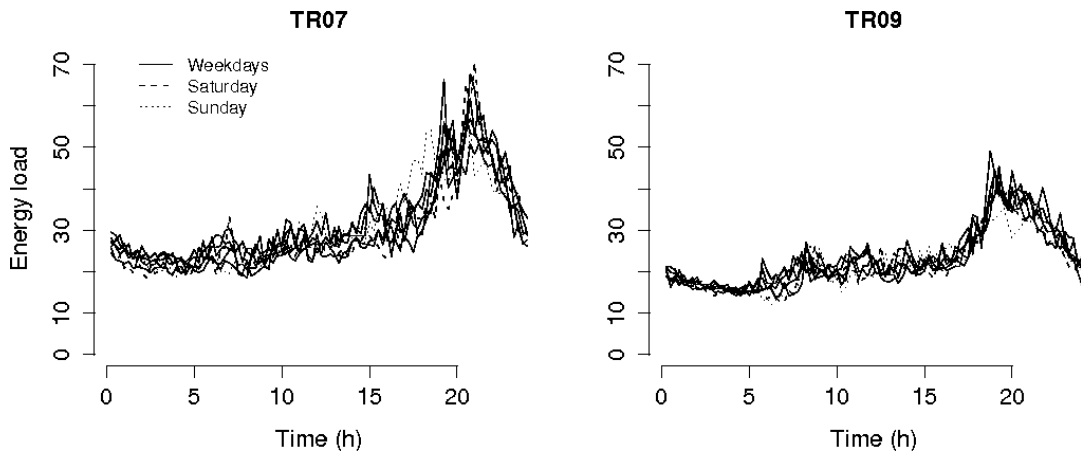

Figure 2.2: Observed curves for two trafos.

Both problems described above can be viewed as examples of samples obtained from aggregated

data; that is, the observed data might be described as a linear combination of individual functional processes and the aim is to estimate their individual mean and covariance functions.

3 Proposed Model

Let $Y_{ij}(t)$ be the j-th replication of curve i observed at point t, $t \in [0, T_F]$. We decompose $Y_{ij}(\cdot)$ as the sum of two components. The first one is described as a weighted sum of C smooth curves, each representing the mean curve of a category c ($c = 1, \cdots, C$). For example, in the electric load example, each disaggregated curve represents the typical curve of consumer type c. The second component represents measurement error, described by a zero mean Gaussian process with some covariance function. More specifically, we assume

$$Y_{ij}(t) = \sum_{c=1}^{C} r_{ic} \alpha_c(t) + \sum_{c=1}^{C} \varepsilon_{ijc}(t), \quad i = 1, \ldots, I, \ j = 1, \ldots, J, \tag{3.1}$$

where $\alpha_1(t), \ldots, \alpha_C(t)$ are the mean curves related to category $c = 1, 2, \cdots, C$, respectively. The r_{ic}s are assumed known and are related to the problem being investigated. These will be discussed in detail in Section 5. We assume $\varepsilon_{ijc}(\cdot)$ follows independent zero mean Gaussian processes with covariance function given by $Z_{ic}(t, s)$, for $t, s \in [0, T_F]$.

In general, the required degree of smoothness depends on the problem under study. However, it is common to require that the functions α_c belong to the Sobolev space $\mathcal{H}_2^2 = \{f : [x_a, x_b] \to \mathbb{R}, \sum_{j=0}^{2} \int (f^{(j)})^2 < \infty\}$. To consider the class $\mathcal{H}_2^2$ as the set of possible mean curves is natural and desirable for this particular situation since it can be well approximated by a finite-dimensional approximating space generated by cubic B-splines, see de Boor (1978). Therefore, the second level of hierarchy expands the mean curves, $\alpha_c(\cdot)$, as a linear combination of B-spline basis. We assume there exists a positive integer K and a knot sequence $\xi = (\xi_1, \cdots, \xi_K)$ such that

$$\alpha_c(t) = \sum_{k=1}^{K} \beta_{ck} B_k(t), \tag{3.2}$$

where $B_k(t)$, $k = 1, \ldots, K$ are cubic B-splines. Consider the function is evaluated at T points, with

$t_1 < t_2 < \cdots < t_T$, following equation (3.2), we can write

$$
\begin{pmatrix} \alpha_c(t_1) \\ \vdots \\ \alpha_c(t_T) \end{pmatrix} = \begin{pmatrix} B_1(t_1) & \cdots & B_K(t_1) \\ \vdots & & \vdots \\ B_1(t_T) & \cdots & B_K(t_T) \end{pmatrix} \begin{pmatrix} \beta_{c1} \\ \vdots \\ \beta_{cK} \end{pmatrix}
\tag{3.3}
$$

for $c = 1, 2, \cdots, C$.

Notice that the design matrix in equation (3.3) does not depend on the category c since we are using the same number of basis and same knot allocation for all categories. Moreover, in this model the coefficients do not depend on the sampled points and all N points of all aggregated curves can be used to estimate the same $C \times K$ coefficients. Therefore, following equation (3.1) and the discussion above, we have the following linear model

$$
Y_{ij}(t) = \sum_{c=1}^{C} \sum_{k=1}^{K} r_{ic} \beta_{ck} B_k(t) + \varepsilon_{ij}(t),
\tag{3.4}
$$

where $\varepsilon_{ij}(t) = \sum_{c=1}^{C} \varepsilon_{ijc}(t)$, because of the independence assumption of $\epsilon_{ijc}(\cdot)$ for $i = 1, \cdots, I$, $j = 1, \cdots, J$, and $c = 1, \cdots, C$. We now discuss in detail the covariance structure among the $\epsilon_{ij}(\cdot)$s.

3.1 Covariance structure of the measurement error

The measurement error captures any structure left after adjusting the data to the sum of the latent disaggregated curves $\alpha_c(.)$. As we are estimating functions we assume the errors are correlated across the domain of $Y_{ij}(\cdot)$.

We expect the correlation between points $Y_{ij}(t)$ and $Y_{ij}(s)$ to decay exponentially, as $|t - s|$ increases. For each category c, we assign an exponential correlation function with decay parameter $\phi_c > 0$ for the Gaussian process associated to each $\epsilon_{ijc}(\cdot)$. Our main contribution lies on the specification of the variance structure. For the i-th curve, let $Z_i(t, s) = \text{Cov}(\varepsilon_{ij}(t), \varepsilon_{ij}(s))$, be the covariance between points t and s. Notice that we assume the same covariance structure across replicates $j = 1, \cdots, J$. We propose the following general structure for $Z_i(t, s)$,

$$
Z_i(t, s) = \sum_{c=1}^{C} C_{ic} \eta_c(t) \, \eta_c(s) \exp(-\phi_c |t - s|),
\tag{3.5}
$$

where $C_{ic}, c = 1, \cdots, C, i = 1, \cdots, I$ are known constants. Like the constants r_{ic} in equation (3.4), the C_{ic}s assume values related to the problem being studied. For every i, we allow the variances to

change with t, such that $Z_i(t,t) = \sum_{c=1}^{C} C_{ic} \eta_c(t)^2$. More generally, the covariance function is allowed to change along the domain of the function. Because of the product $\eta_c(t) \, \eta_c(s)$ in equation (3.5) we do not need to impose any particular restriction on the $\eta_c(\cdot)$s to guarantee that we have a valid covariance function. It is worth noting that this covariance function might assume negative values, depending solely on the function $\eta_c(\cdot)$.

We consider three different models for the components $\eta_c(\cdot)$s:

(a) **Uniformly homogeneous case**: In this case we assume

$$\eta_c(t) = \sigma, \ \forall \, t \quad \text{and} \quad \phi_c = \phi,$$

implying that $Z_i(t,s) = (\sum_{c=1}^{C} C_{ic}) \sigma^2 \exp(-\phi|t-s|)$, for all $c = 1, \ldots, C$.

(b) **Homogeneous case**: Here we relax the assumption of common σ^2 and ϕ by assuming

$$\eta_c(t) = \sigma_c, \ \forall \, t,$$

which leads to $Z_i(t,s) = \sum_{c=1}^{C} C_{ic} \sigma_c^2 \exp(-\phi_c|t-s|)$, i.e.

(c) **Heterogenous case**: The more general case expands $\eta_c(\cdot)$ in B-splines basis functions, such that

$$\eta_c(t) = \sum_{\ell=1}^{L} \theta_{c\ell} B_\ell(t), \tag{3.6}$$

where $B_\ell(t), \ell = 1, \cdots, L$ are cubic B-splines with (possibly) a different knot sequence from that for $\alpha_c(\cdot)$, say ξ_η, and the covariance function follows the general structure shown in Equation (3.5).

3.2 Likelihood function and Prior specification

Assume $\mathbf{y}$ represents the IJT-dimensional vector of observations, with components $\mathbf{y} = (y_{11}(t_1), \cdots, y_{1J}(t_1), \cdots, y_{11}(t_T), \cdots, y_{1J}(t_T), \cdots, y_{IJ}(t_T))$. Considering the more general case, denote by $\boldsymbol{\Theta}$ the parameter vector for the model. We will specify this vector for the three covariance structures considered. Notice that for each $i = 1, \cdots, I$, and $j = 1, \cdots, J$, conditioned on the parameter vector, $\mathbf{Y}_{ij} = (Y_{ij}(t_1), \cdots, Y_{ij}(t_T))'$ follows independent normal distributions such that

$$\mathbf{Y}_{ij} \sim N_T(X_i \boldsymbol{\beta}, Z_i), \tag{3.7}$$

10

where X_i are $T \times CK$ matrices given by

$$X_i = \begin{pmatrix} r_{i1}B_1(t_1) & \cdots & r_{i1}B_K(t_1) & \cdots & r_{iC}B_1(t_1) & \cdots & r_{iC}B_K(t_1) \\ \vdots & \cdots & \vdots & \cdots & \vdots & \cdots & \vdots \\ r_{i1}B_1(t_T) & \cdots & r_{i1}B_K(t_T) & \cdots & r_{iC}B_1(t_T) & \cdots & r_{iC}B_K(t_T) \end{pmatrix},$$

$\boldsymbol{\beta} = (\boldsymbol{\beta}_1, \cdots, \boldsymbol{\beta}_C)'$, with $\boldsymbol{\beta}_c = (\beta_{c1}, \cdots, \beta_{cK})'$, is the CK dimensional vector of coefficients, and $Z_i = Z_i(\boldsymbol{\Theta})$ are covariance matrices of order T with elements given by Equation (3.5). Therefore, based on the observed vector $\mathbf{y}$, the likelihood function for $\boldsymbol{\Theta}$ can be written as

$$L(\boldsymbol{\Theta}; \mathbf{y}) \propto \prod_{i=1}^{I} \prod_{j=1}^{J} |Z_i|^{-1/2} \exp\left\{ -\frac{1}{2}(\mathbf{y}_{ij} - X_i\boldsymbol{\beta})' Z_i^{-1} (\mathbf{y}_{ij} - X_i\boldsymbol{\beta}) \right\}. \tag{3.8}$$

As our inference procedure follows the Bayesian paradigm, we now specify the prior distribution of the parameter vector $\boldsymbol{\Theta}$ depending on the covariance structure.

Prior specification   We assume prior independence among the components of the parameter vector $\boldsymbol{\Theta}$. In particular, for the coefficients $\boldsymbol{\beta}_c$ we assign K-dimensional multivariate normal distributions with known mean vector $\mathbf{b}_c$ and covariance matrice Ω_c, $c = 1, 2, \cdots, C$. In Section 5 we assume a zero mean prior for $\boldsymbol{\beta}_c$. However, experts in the field of interest might provide useful information about the shape of each function, and this can be induced through the mean of the prior distributions of the respective $\boldsymbol{\beta}_c$s. For the covariance matrices Ω_c we assume diagonal matrices, with the diagonal elements fixed at some large value to let the observed data drive the inference procedure. The prior specification of the parameters in the covariance function is related to the choice of the covariance structure proposed in Section 3.1.

(a) **Uniformly homogeneous case:** in this case the parameter vector is defined as $\boldsymbol{\Theta}^U = (\boldsymbol{\beta}, \sigma^2, \phi)$. For σ^2 we assume an inverse gamma distribution with shape parameter d and rate parameter l. For ϕ, we assign a gamma prior distribution with shape parameter p and rate parameter q fixed at some reasonable value. For example, we can use the idea of practical range. The mean of the prior, p/q can be fixed such that at a reasonable distance, the correlation is close to zero, say 0.05. More specifically, we fix the mean at the value that solves $0.05 = \exp(-\phi^* dist)$, where ϕ^* is the prior mean guess we need, and $dist$ is a fixed distance.

(b) Homogeneous case: for the homogenous covariance structure we define the parameter vector as $\boldsymbol{\Theta}^H = (\boldsymbol{\beta}, \sigma_1^2, \sigma_2^2, \cdots, \sigma_C^2, \phi_1, \phi_2, \cdots, \phi_C)$. We suggest independent inverse gamma prior distributions, each with parameters (d_c, l_c), for each σ_c^2. We also assume prior independence among the decay parameters ϕ_c of the exponential correlation function; and each one is assumed to follow a gamma prior distribution with parameters p_c and q_c, $c = 1, \cdots, C$, with p_c and q_c fixed at some reasonable values. The same idea of practical range discussed in the uniformly homogenous case can be used here.

(c) Heterogeneous case: the parameter vector to be estimated is $\boldsymbol{\Theta}^{NH} = (\boldsymbol{\beta}, \boldsymbol{\theta}_1, \cdots, \boldsymbol{\theta}_C, \phi_1, \cdots, \phi_C)$. We assume independent K-dimensional multivariate normal prior distributions for the coefficients $\boldsymbol{\theta}_c$, each with known mean vector $\mathbf{d}_c$, and covariance matrix Λ_c. Like in the mean values of $\boldsymbol{\beta}$, the $\mathbf{d}_c$s can be obtained by experts in the field. However, it might be more challenging to elicitate these values as they are in the covariance structure of the process. For the covariance matrices Λ_c we assume diagonal matrices, with the diagonal elements fixed at some reasonably large value to let the observed data drive the inference procedure.

Posterior distribution and inference procedure   Following the Bayesian paradigm, the posterior distribution, $p(\boldsymbol{\Theta} \mid \mathbf{y})$, is proportional to the likelihood function times the prior distribution of $\boldsymbol{\Theta}$.

The resultant posterior distributions under all different covariance functions do not have closed forms. We use Markov chain Monte Carlo (MCMC) methods, specifically, the Gibbs sampler with some steps of the Metropolis-Hastings (M-H) algorithm to obtain samples from the target posterior distribution (see e.g. Gamerman and Lopes (2006)). In particular, the full conditional posterior distributions of $\boldsymbol{\beta}_c$ are normal distributions, which are easy to sample from. Independent of the assumed covariance function, the full conditional posterior distributions of each of the parameters involved in it do not result in known distributions. For these parameters we make use of the Metropolis-Hastings algorithm with log-normal proposals based on the current value of the chain, and some fixed variance, tuned to give reasonable acceptance rates. The MCMC algorithm was implemented in R (R Development Core Team, 2010), and the codes are available from the authors upon request.

3.3 Predictive inference

From a Bayesian point of view, one can obtain the posterior predictive distribution of the function $Y_i(\cdot)$ at unobserved values of the domain of the function, $\mathbf{Y}_i^* = (Y_i(t_1^*), \cdots, Y_i(t_L^*))$, for $t_l^* \in [0, T_F]$, $l = 1, \cdots, L$, through

$$p(\mathbf{y}_i^* \mid \mathbf{y}) = \int_{\Theta} p(\mathbf{y}_i^* \mid \mathbf{y}, \Theta) p(\Theta \mid \mathbf{y}) d\Theta. \tag{3.9}$$

The model assumes that samples $Y_i(\cdot)$ are being generated from the multivariate normal distribution, $N(X_i\boldsymbol{\beta}, Z_i)$. From the theory on the multivariate normal distribution (Anderson, 1984), it follows that the joint distribution of $\mathbf{Y}$ and $\mathbf{Y}_i^*$, conditioned on Θ, is given by

$$\left(\begin{array}{c} \mathbf{Y}_i^* \\ \mathbf{Y} \end{array} \middle| \Theta \right) \sim N \left(\left(\begin{array}{c} X_i^*\boldsymbol{\beta} \\ X_i\boldsymbol{\beta} \end{array} \right) ; \left(\begin{array}{cc} Z_i^* & Z_{i_{12}}' \\ Z_{i_{12}} & Z_i \end{array} \right) \right), \tag{3.10}$$

where X_i^* is a L-dimensional vector with elements equal to the cubic B-splines at point t_l^*; X_i is a vector comprising the cubic B-splines at the observed points t_t; Z_i^* is a covariance matrix of dimension L and each of its element is the covariance of the process between unobserved points. Each line of the matrix $Z_{i_{12}}$, $T \times L$, represents the covariance between the ith observed point and the jth unobserved one, $i = 1, \cdots, T$ and $j = 1, \cdots, L$. From the theory of the multivariate normal distribution we have that

$$\mathbf{Y}_i^* | \mathbf{y}_i, \Theta \sim N_L \left(X_i^*\boldsymbol{\beta} + Z_{i_{12}}' Z_i^{-1} \left(\mathbf{y}_i - X_i\boldsymbol{\beta} \right) ; Z_i^* - Z_{i_{12}}' Z_i^{-1} Z_{i_{12}} \right). \tag{3.11}$$

The integration in (3.9) does not have an analytical solution, however approximations can be easily obtained through Monte Carlo methods (Gamerman and Lopes, 2006). For each sample s, $s = 1, \cdots, Q$, obtained from the MCMC algorithm, we can obtain an approximation for (3.9), by sampling from the distribution in (3.11) and computing

$$p(\mathbf{y}_i^* | \mathbf{y}) \approx \frac{1}{Q} \sum_{s=1}^{Q} p(\mathbf{y}_i^* | \Theta^s). \tag{3.12}$$

Once samples from the posterior distribution of Θ are available, realizations from the posterior predictive distribution can be obtained by sampling from the distribution of $\mathbf{Y}_i^* \mid \mathbf{y}, \Theta^s$, with Θ^s representing the sth sampled parameter vector Θ.

4 Analyzing artificial data sets

Here we analyze six artificial sets of data to check the ability of the model in estimating the disaggregated curves of interest when the truth is known. All datasets assume $C = 2$ population curves. We consider data are generated from

$$Y_{ij}(t) = r_{i1}\alpha_1(t) + r_{i2}\alpha_2(t) + \epsilon_{ij}(t), \quad i = 1, 2, 3, \; j = 1, \cdots, J, \quad (4.1)$$

where the true curves are given by

$$\begin{aligned}
\alpha_1(t) &= 5\exp\{-t\}\sin(\pi\,t/2)\cos(\pi\,t) \\
\alpha_2(t) &= 5\exp\{-(t - 0.2)\}\cos(\pi\,t/2)\sin(\pi\,t),
\end{aligned}$$

with $r_{11} = 1$, $r_{12} = 4$, $r_{21} = 4$, $r_{22} = 1$, $r_{31} = 2.5$ and $r_{32} = 2.5$. These curves were chosen because they have interesting features to be captured by the model. We explore 6 different scenarios by assuming different specifications for the covariance structures of $\epsilon_{ij}(\cdot)$:

Case 1: Uniformly homogeneous case In this case we assume all $C_{ic} = 1$, $\sigma^2 = 1$ and $\phi = 0.5$. We concetrated on the case where there are no replicates for the aggregated curves, such that $J = 1$ and we obtained samples for $I = 10$ and $I = 30$.

Case 2: Homogeneous case Here we assume

$$Z_i(t, s) = C_{i1}\sigma_1^2 \exp(-\phi_1|t - s|) + C_{i2}\sigma_2^2 \exp(-\phi_2|t - s|), \quad (4.2)$$

and we fix the parameters at the following values: $\sigma_1^2 = \sigma_2^2 = 1$, $\phi_1 = \phi_2 = 4$ and $C_{11} = 1$, $C_{12} = 1.3$, $C_{21} = 1.4$, $C_{22} = 1.3$, $C_{31} = 1.5$ and $C_{32} = 1.5$. Here we consider only the case $J = 15$.

Case 3: Heterogeneous case Here we assume

$$Z_i(t, s) = C_{i1}\eta_1(t)\eta_1(s) \exp(-\phi_1|t - s|) + C_{i2}\eta_2(t)\eta_2(s) \exp(-\phi_2|t - s|) \quad (4.3)$$

with η_1 and η_2 curves generated as linear combinations of B-splines, $\phi_1 = \phi_2 = 4$ and $C_{11} = 1$, $C_{12} = 1.3$, $C_{21} = 1.4$, $C_{22} = 1.3$, $C_{31} = 1.5$ and $C_{32} = 1.5$. For the heterogeneous covariance structure we fit the model considering $J = 15$, $J = 50$ and $J = 150$. This is to investigate the

14

effect of the number of replicates on the estimates of the parameters when a more flexible covariance structure is assumed.

For all datasets we assumed 14 B-splines basis with $K = 10$ internal knots. In the heterogeneous case, we assumed this same set of knots to estimate $\eta_1(.)$ and $\eta_2(.)$. We let the MCMC algorithm run for 100,000 iterations, considered the first 5,000 as burn-in and kept every 95-th sample to avoid autocorrelation between the sampled values. Convergence of the chains was checked through the use of two chains starting from very different values.

For the uniformly homogeneous case we notice that inspite of the value of I the posterior distribution of σ^2 and ϕ seem to recover the true values used to generated the data. On the other hand, the value of I seems to have influence on the magnitude of the ranges of the 95% posterior credible intervals of the disaggegated curves $\alpha_c(\cdot)$ (Figures 4.1 and 4.2).

For the homogeneous case, even with only $J = 15$ replicates, the model is able to recover the true structure of the disaggregated functions $\alpha_1(.)$ and $\alpha_2(.)$. The posterior mean of both curves are very close to their respective true values and the range of the 95% posterior credible intervals are relatively narrow. The parameters in the covariance structure are also well estimated (Figure 4.3).

For the heterogenous case it is clear that the number of replicates affect the range of the posterior credible intervals both for $\alpha_c(.)$ and $\eta_c(.)$, $c = 1, 2$. Regardless of the value of J the true values are recovered from the inference procedure, specially for the disaggregated functions $\alpha_c(.)$. The greater the number of replicates the narrower the 95% posterior credible intervals (Figures 4.4 and 4.5). The true values of the decay parameters ϕ_1 and ϕ_2 are also recovered from the inference procedure, and similar to the results for $\alpha_c(.)$ and $\eta_c(.)$, the magnitude of J influences the range of the posterior credible intervals (Figure 4.6).
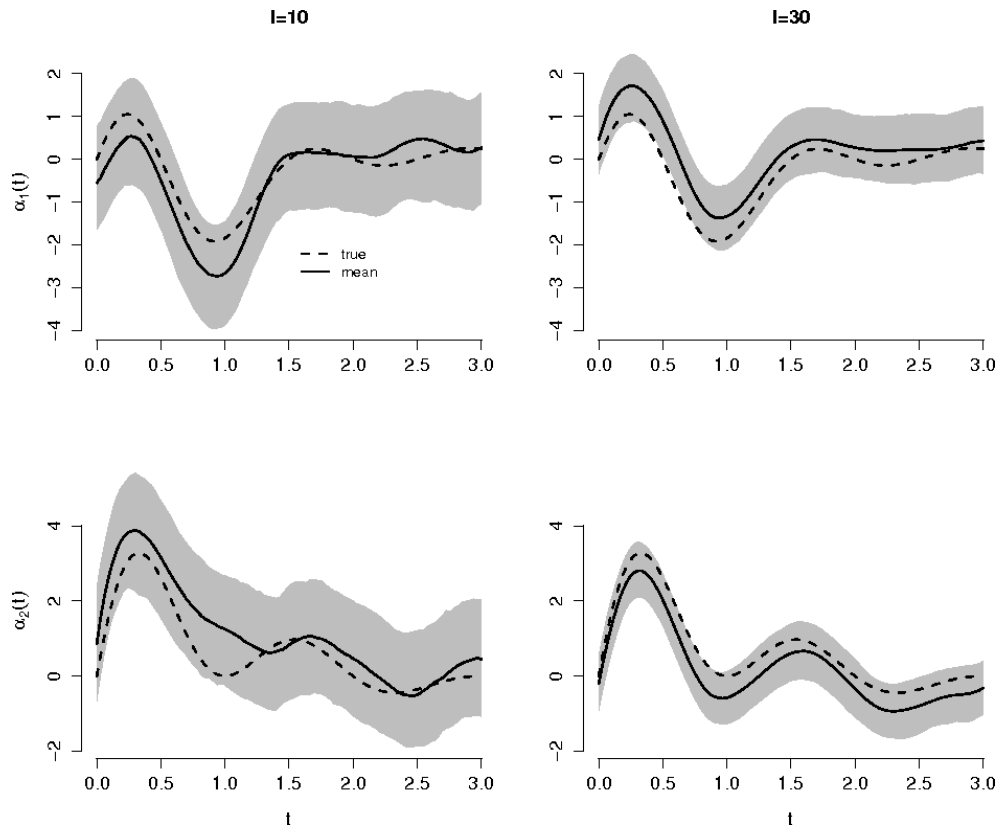
Figure 4.1: Summary of the posterior distribution of the parameters for the uniformly homogeneous case with $J = 1$, $I = 10$ (first column) and $I = 30$ (second column). Posterior mean curves (solid lines) and limits (shaded area) of the 95% posterior credible intervals. Dashed lines represent respective true values.
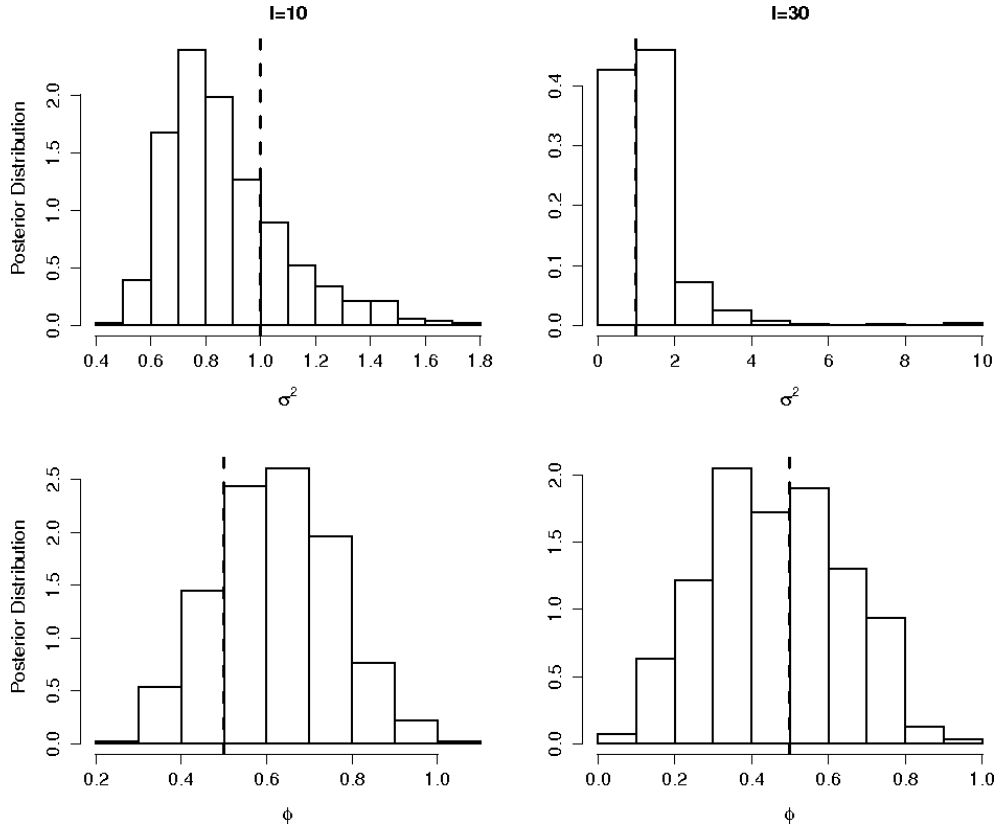
16

Figure 4.2: Summary of the posterior distribution of the parameters for the uniformly homogeneous case with $J = 1$ and $I = 10$ (first row) and $I = 30$ (second row). Posterior distribution of σ^2 and and ϕ. Dashed lines represent respective true values.
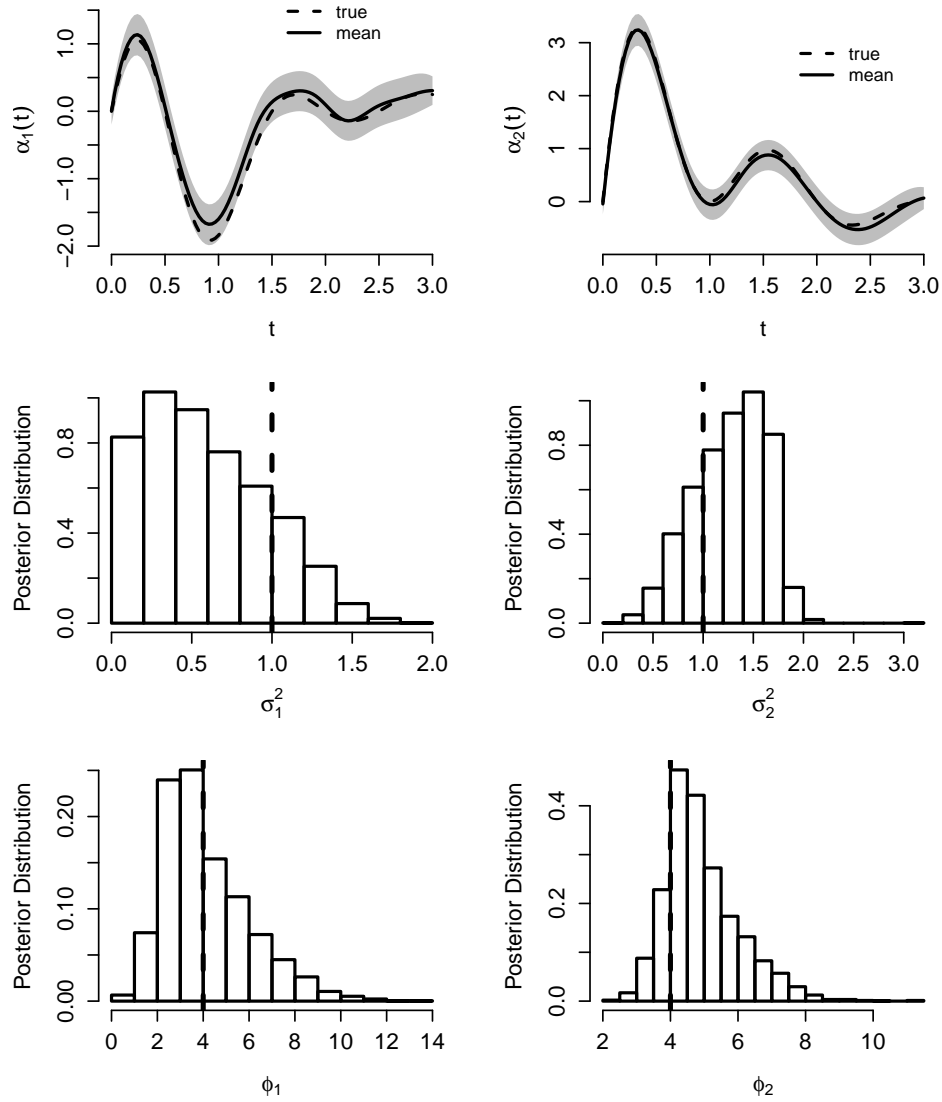
Figure 4.3: Summary of the posterior distribution of the parameters for the homogeneous case with $J = 15$. Posterior mean curves (solid lines) and limits (shaded area) of the 95% posterior credible intervals (1st row), posterior distribution of σ_1^2 and σ_2^2 (2nd row), and ϕ_1 and ϕ_2 (3rd row). Dashed lines represent respective true values.
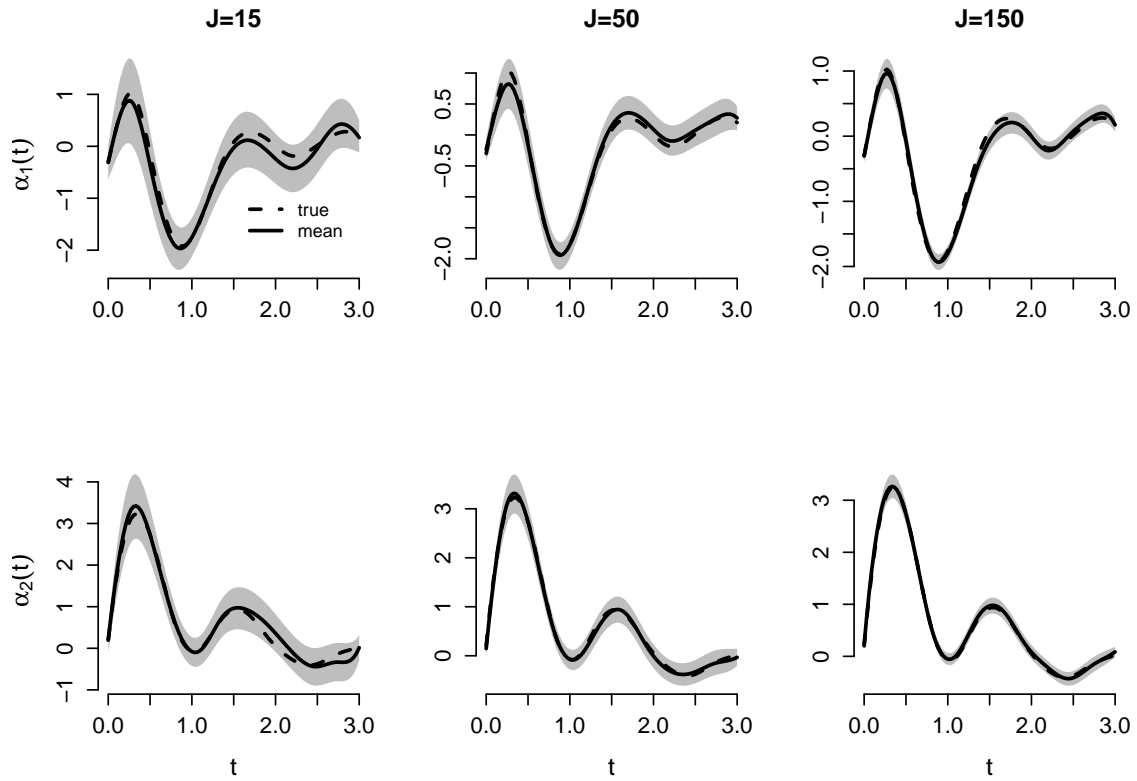
Figure 4.4: Posterior mean curves (solid lines) and limits (shaded area) of the 95% posterior credible intervals for (a) $\alpha_1(.)$, $J = 15$, (b) $\alpha_2(.)$, $J = 15$, (c) $\alpha_1(.)$, $J = 50$, (d) $\alpha_2(.)$, $J = 50$, (e) $\alpha_1(.)$, $J = 150$, (f) $\alpha_2(.)$, $J = 150$. In all panels the dashed line is the respective true curve.

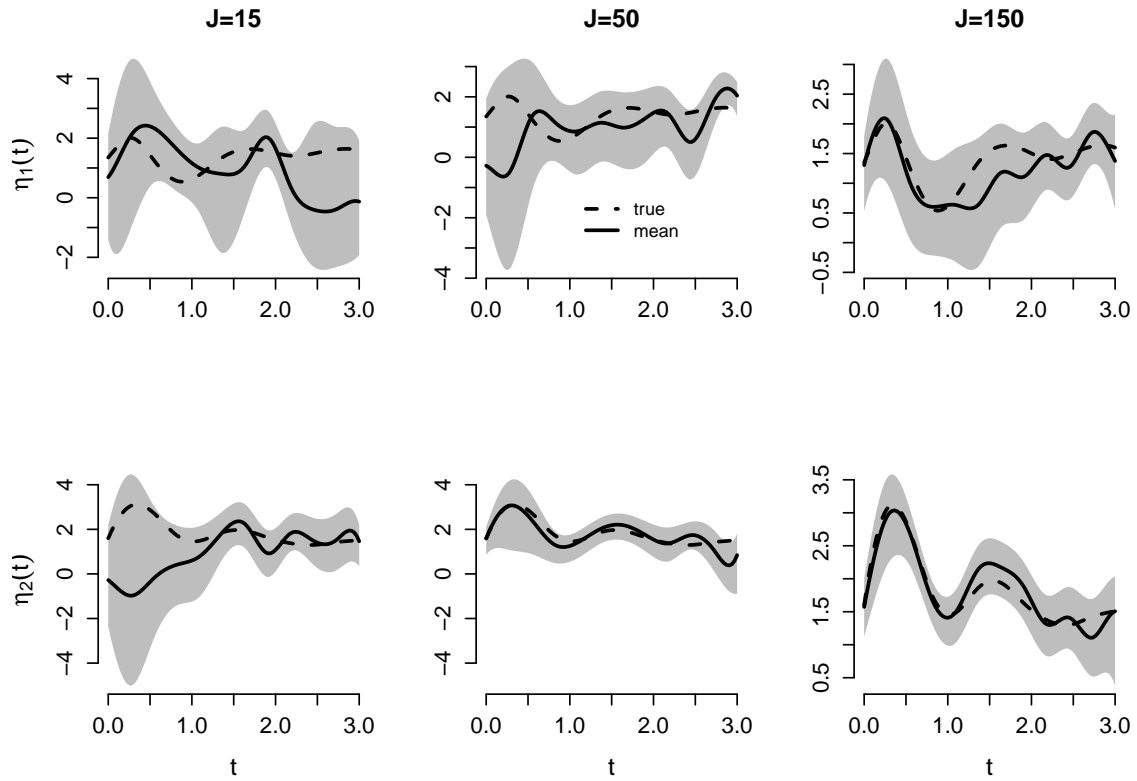Figure 4.5: Posterior mean (solid line) of the variance functions $\eta_1(.)$ and $\eta_2(.)$ (rows) and limits (shaded area) of the 95% posterior credible intervals for the heterogeneous case with $J = 15$, $J = 50$ and $J = 150$ (columns). The dashed lines represent the true curves used to generate the data.
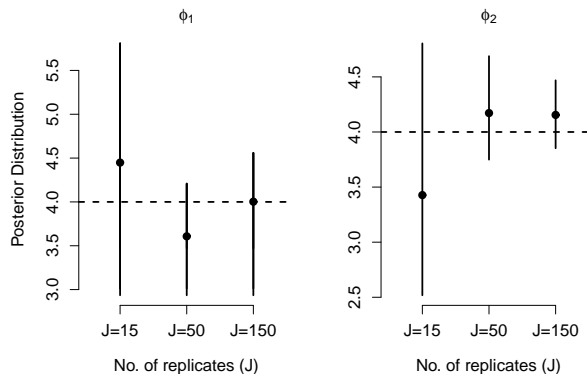
Figure 4.6: Posterior summary (solid circle: posterior mean and lines represent the limits of the 95% posterior credible intervals) of the decay parameters ϕ_1 and ϕ_2 in equation (3.5). Dashed line represents true value used to generate the data.

5 Applications

5.1 NIR Spectroscopy data - Polyaromatic hydrocarbons

The Beer-Lambert law for K constituents plus noise states that for the ith chemical sample the measurement at wavelength t is given by

$$Y_i(t) = \sum_{\ell=1}^{C} r_{\ell,i}\alpha_\ell(t) + \sum_{\ell=1}^{C} e_{\ell,i}(t), \quad t \in [220, 350], \quad i = 1, \ldots, 25. \tag{5.1}$$

where $r_{\ell,i}$ is the concentration of the ℓ constituent in the ith chemical sample , $\alpha_\ell(t)$ is the absorbance at wavelength t of the ℓth pure constituent and $e_{\ell,i}$ is a random noise.

Notice that the Beer-Lambert formula leads exactly to the functional model of aggregated data given by Equation (1.1).

In this example, we used 14 B-spline basis with 10 internal knots equally spaced in the interval (220,350) to estimate the latent absorbance curves of each constituint, $\alpha_c(\cdot)$.

Since there are no replicates of the population curves available and we have $C = 10$ constituints, we chose to fit the model considering a homogeneous covariance structure. In this case, we used a gamma prior for ϕ_c, and an inverse gamma with parameters 2 and 0.2 for σ_c^2, $c = 1, \ldots, 10$. We let the MCMC algorithm run for 100,000 iterations, considered the first 5,000 as burn-in and kept every 100-th sample to avoid autocorrelation between the sampled values.
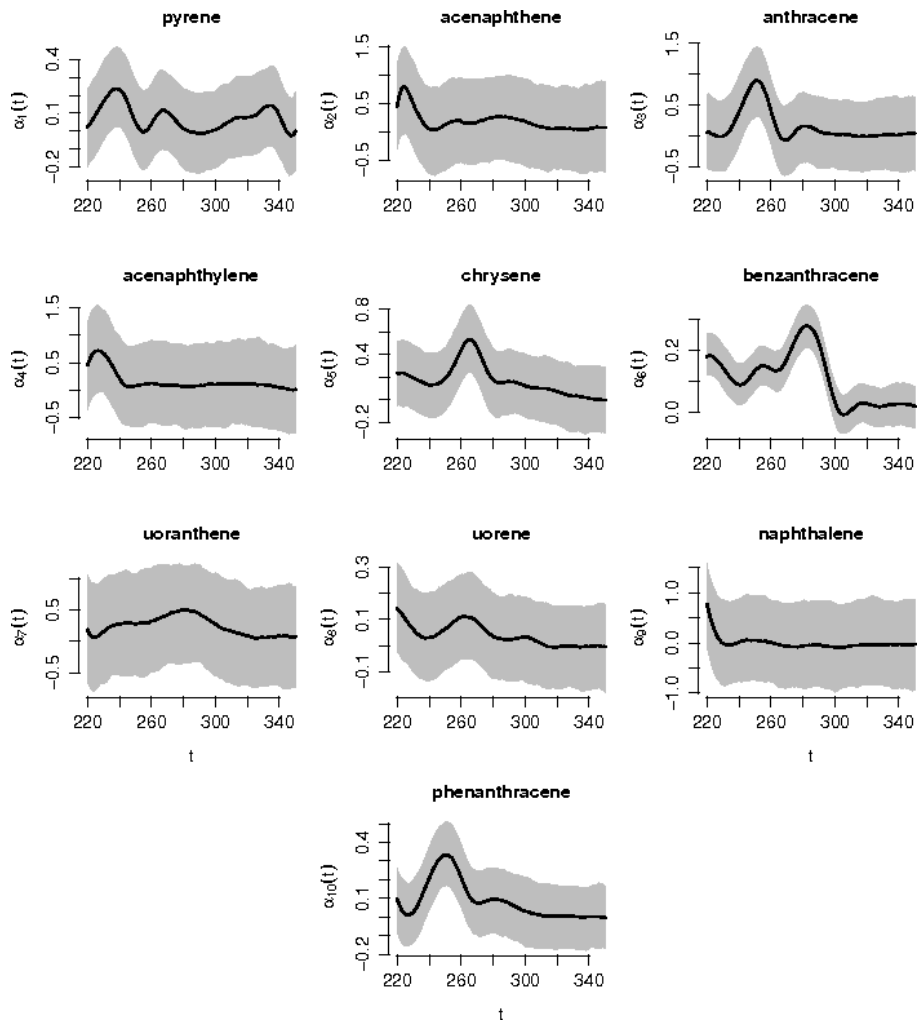

Figure 5.1: Estimated absorbance curves for the constituints, for the PAH dataset under the uniformly homogeneous model.

Figure 5.1 shows the estimated individual curves for each of the constituints. However, to see how good these estimates are we should compare the aggregated observed curves with the weighted sum of these estimates using the Beer-Lambert formula. These comparisons are made in Figures 5.2 and 5.3. The confidence bands for Figure 5.2 are the quantiles weighted sum of the estimates whereas Figure 5.3 compares the data obtained in some chemical samples with the predictive 95% confidence intervals. Both figures show that we have an excelent fit for the data.
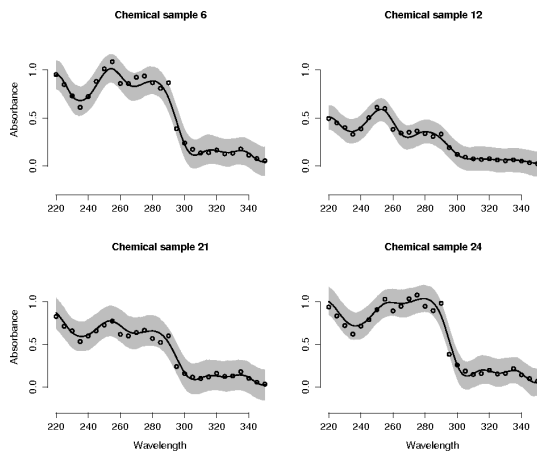

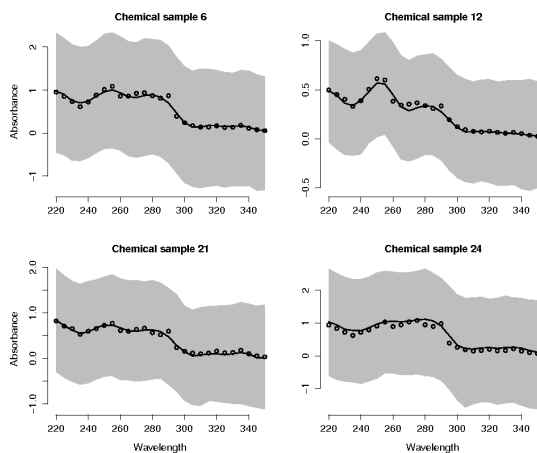Figure 5.2: Estimated curves for chemical samples 6, 12 ,21 and 24

Figure 5.3: Predictive 95% confidence intervals for chemical samples 6, 12 ,21 and 24

5.2 Electric load data

Here we analyze electric load data as described in Section 2.2. In Brazil, for security reasons, houses are loaded with energy tension either equal to 127V or 220V. For this reason, they are classified as monophasic (single phase/ 127V) or biphasic (two phases/220V). Usually, more modest residencies are monophasic suggesting that monophasic and biphasic consumers have different typologies. We consider samples observed from $I = 2$ trafos which are denoted by TR07 and TR09. The market for each trafo is small and variable, consisting only of single phase and two phase residential consumers. The consumption of energy during weekends is different than from weekdays (Figure 2.2). Therefore, we decide to analyse only the weekdays resulting that $J = 5$ replicates.

Measurements from trafos TR07 and TR09 were stored at every 15 minutes, during 5 days of a particular week. It is known that the electric load of each trafo i is equal to the sum of $N_i = N_{i1} + N_{i2}$ curves, where N_{ic} is the number of consumers of type c (monophasic or biphasic here), and (N_{i1}, N_{i2}) is the market of trafo i. Table 5.1 presents the number of consumers (market) for each trafo.

Trafo	Single Phase	Two Phase	Total
TR07	87	5	92
TR09	25	25	50

Table 5.1: Distribution of the number of consumers (market) for trafos TR07 and TR09 in the electric load application.

Following the general structure in equation (3.1), we model the traffic load of trafo i, at day j, observed at time t as

$$Y_{ij}(t) = \sum_{c=1}^{C} \sum_{n_c=1}^{N_{ic}} W_{cjn_ci}(t), \quad t \in [0, 24], \quad i = 1, 2, \quad j = 1, \ldots, 5, \tag{5.2}$$

where $W_{c,j,n_c,i}(t) = \alpha_c(t) + \varepsilon_{c,j,n_c,i}(t)$. For this example the constants r_{ic} and C_{ic} (in equations (3.4) and (3.5)) coincide and are equal to N_{ic}.

We fitted the model assuming 14 B-spline basis, with $K = 10$ internal knots located at the following points $\xi = \{4, 6, 8, 10, 12, 14, 16, 18, 19, 20\}$. We fitted the model considering a heterogeneous covariance structure. The prior specification of ϕ_c uses the idea of practical range as discussed in

Section 3.2. *A priori*, we assume the correlation between measurements in a day dies off, in average, after 3/4 of an hour. We assume a gamma prior for ϕ_c with mean equals $3/0.75 = 4$, and variance 1. Panels of figure 5.4 show the posterior mean with respective 95% posterior credible intervals for the mean and variance curves for monophasic and biphasic consumers. As expected the single phase houses have a smaller load than the two phase residencies. Both types have a peak around 8pm, as this coincides with arriving home from work, taking showers, etc. The basic difference is that for two phase residencies there is an increase in the electric load from 8am to 12pm which is not observed for the single phase consumers.
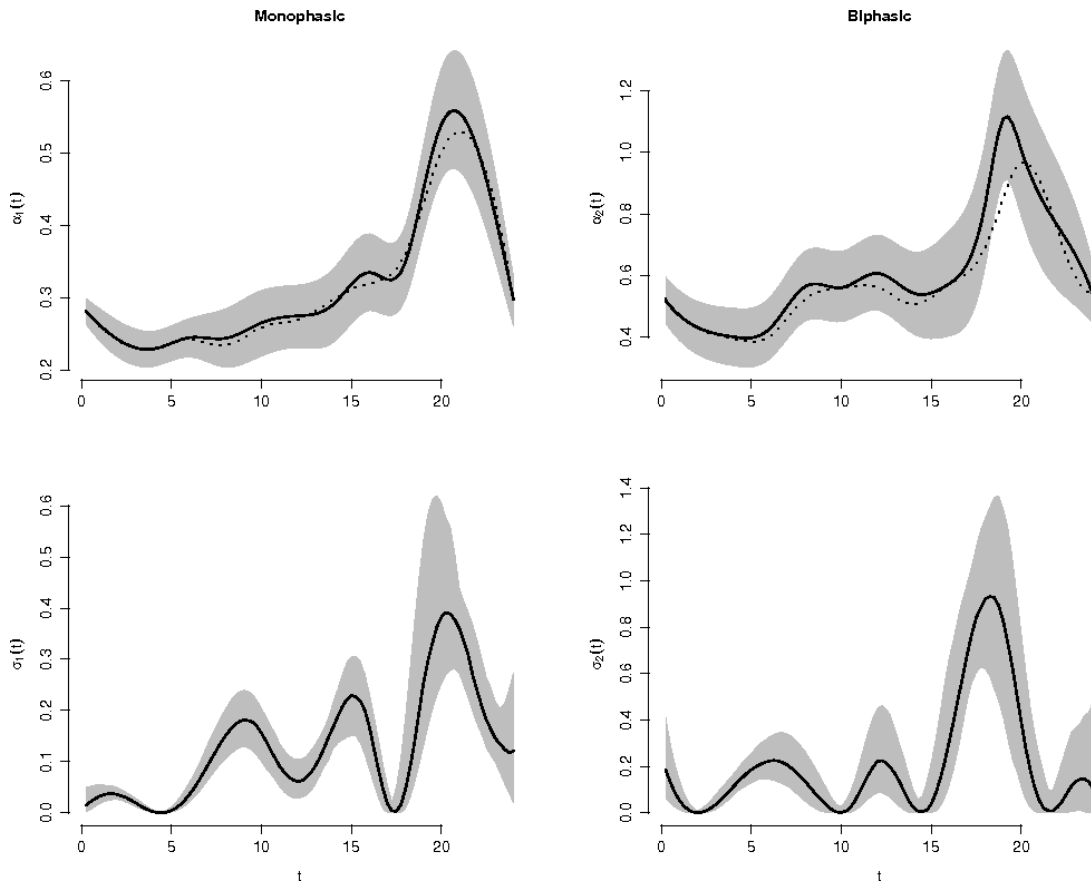

Figure 5.4: Posterior mean (solid line) and 95% credible intervals (shaded area) for monophasic (single phase) and biphasic (two phase) consumers based on trafos TR07 and TR09 for the tipologies (first row) and variance (second row). The dotted lines in the first row show the estimate obtained under the frequentist approach proposed by Dias et al (2009).

Figure 5.5 compares the posterior predictive distribution with the observations. It is clear that the proposed model is capturing quite well the structure of the data, as most of the observations are within the limits of the 95% posterior predictive interval.
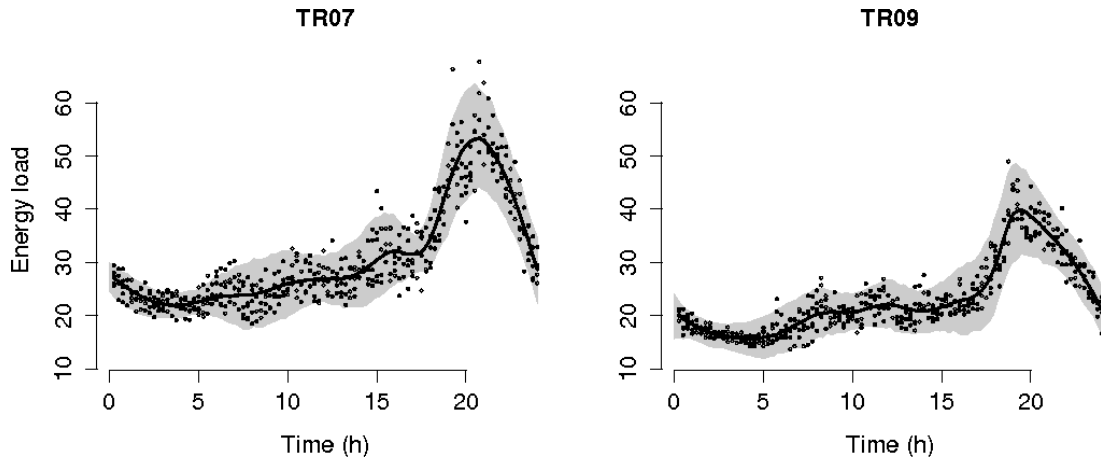

Figure 5.5: Summary of the posterior predictive distribution (solid lines) and limits of the 0.025 and 0.975 quantile curves (shaded area) compared with the respective observed values (hollow circles), for trafos TR07 and TR09.

6   Concluding remarks

In this work our attention was focused on the Bayesian estimation of latent sub-population (disaggregated) mean and covariance curves when we only have available observations of the population (aggregated) curves. Although our proposed models are an extension of the model initially proposed by Dias et al. (2009), we propose more flexible nonstationary covariance structures for the Gaussian process by allowing the variance of the process to change across the domain of the function. The general non-parametric case naturally imposes the positive definiteness of the covariance function and can be restricted to accomodate many different situations. We believe our proposed covariance structure might also be applied in different areas, e.g. geostatistics.

There are several advantages of using the Bayesian paradigm:

- It might naturally incorporate prior information that is available to experts in the field;

- Estimates are obtained under a single framework;

- and it naturally provides the uncertainties of the estimates of the latent sub-population curves, not only of the mean curves but also of the covariance curves.

To show the strength of our method, we analyzed two examples from different areas in science: environmetrics and chemometrics. In both examples it is clear, from comparing the observed aggregated curves with the weighted sum of the estimated latent ones, that the proposed model provide extremely reasonable estimates.

References

Anderson, T. (1984). *An Introduction to Multivariate Statistical Analysis*, John Wiley & Sons, Inc.

Botonjic-Sehic, E., Brown, C. W., Lamontagne, M. and Tsaparikos, M. (2009). Forensic application of near-infrared spectroscopy: Aging of bloodstains, *Spectroscopy*, February 2009, http://spectroscopyonline.findanalytichem.com/spectroscopy/Near-IR+Spectroscopy/Forensic-Application-of-Near-Infrared-Spectroscopy/ArticleStandard/Article/detail/583780.

Brereton, R. (2003). *Chemometrics: Data Analysis For the Laboratory and Chemical Plant*, Wiley, Chichester.

Candolfi, A., De Maesschalck, R., Massart, D. L., Hailey, P. A. and Harrington, A. (1999). Identification of pharmaceutical excipients using NIR spectroscopy and simca., *J. Pharm. Biomed. Anal.* **19**(6): 923–935.

Cozzolino, D., Flood, L., Bellon, J., Gishen, M. and De Barros Lopes, M. (2006). Combining near infrared spectroscopy and multivariate analysis as a tool to differentiate different strains of *saccharomyces cerevisiae*: a metabolomic study, *Yeast* **23**(14–15): 1089–1096.

de Boor, C. (1978). *A Practical Guide to Splines*, Springer Verlag, New York.

Dias, R. (1998). Density estimation via hybrid splines, *J. Statist. Comput. Simul.* **60**: 277–294.

Dias, R. (2000). A note on density estimation using a proxy of the Kullback-Leibler distance, *Braz. J. Prob. Stat.* **13**(2): 181–192.

Dias, R., Garcia, N. L. and Martarelli, A. (2009). Non-parametric estimation for aggregated functional data for electric load monitoring, *Environmetrics* **20**(2): 111–130.

Eubank, R. (1999). *Nonparametric Regression and Spline Smoothing*, number 157 in *Statistics: textbooks and monographs*, 2nd edn, Dekker, New York, NY, USA.

Gamerman, D. and Lopes, H. F. (2006). *Monte Carlo Markov Chain: Stochastic Simulation for Bayesian Inference*, Chapman and Hall, London.

Kooperberg, C. and Stone, C. J. (1991). A study of logspline density estimation, *Comp. Stat. Data Anal.* **12**: 327–347.

Maraboli, A., Cattaneo, T. M. P. and Giangiacomo, R. (2002). Detection of vegetable proteins from soy, pea and wheat isolates in milk powder by near infrared spectroscopy, *J. Near Infrared Spectrosc.* **10**(1): 63–69.

R Development Core Team (2010). *R: A Language and Environment for Statistical Computing*, R Foundation for Statistical Computing, Vienna, Austria. ISBN 3-900051-07-0.

Rodriguez-Saona, L. E., Khambaty, F. M., Fry, F. S. and Calvey, E. M. (2001). Rapid detection and identification of bacterial strains by Fourier transform near-infrared spectroscopy, *J. Agric. Food Chem.* **49**(2): 574–579.

Romía, M. B. and Bernárdez, M. A. (2010). NIR spectroscopy in pharmaceutical analysis: Off-line and at-line PAT applications, *in* K. Bakeev (ed.), *Process Analytical Technology: Spectroscopic Tools and Implementation Strategies for the Chemical and Pharmaceutical Industries*, John Wiley & Sons, Ltd, Chichester, UK, pp. 463–491.

Saranwong, S. and Kawano, S. (2008a). Interpretation of near infrared calibration structure for determining the total aerobic bacteria count in raw milk: interaction between bacterial metabolites and water absorptions, *J. Near Infrared Spectrosc.* **16**(6): 497–504.

Saranwong, S. and Kawano, S. (2008b). System design for non-destructive near nfrared analyses of chemical components and total aerobic bacteria count of raw milk, *J. Near Infrared Spectrosc.* **16**(4): 389–398.

Schönbrodt, T., S., M., Winter, G. and G., R. (2006). NIR spectroscopy-a non-destructive analytical tool for protein quantification within lipid implants., *J. Controlled Release* **114**(2): 261–267.

Silverman, B. W. (1986). *Density Estimation for Statistics and Data Analysis*, Chapman and Hall (London).

Tewari, J., Mehrotra, R. and Irudayaraj, J. (2003). Direct near infrared analysis of sugar cane clear juice using a fibre-optic transmittance probe, *J. Near Infrared Spectrosc.* **11**(5): 351–356.

Vidakovic, B. (n.d.). *Statistical Modeling by Wavelets*, Wiley Series in Probability and Statistics: Applied Probability and Statistics.

Woodcock, T., O'Donnell, C. P. and Downey, G. (2008). Review: Better quality food and beverages: the role of near infrared spectroscopy, *J. Near Infrared Spectrosc.* **16**(1): 1–29.